RESEARCH MEMORANDUM

A SEMIGRAPHICAL METHOD FOR THE DETERMINATION OF THE ROLLING CHARACTERISTICS OF ROLLERON-EQUIPPED MISSILES

By Martin L. Nason

Langley Aeronautical Laboratory
Langley Field, Va.

NATIONAL ADVISORY COMMITTEE
FOR AERONAUTICS

WASHINGTON

November 29, 1956

NACA RM L56I12

NATIONAL ADVISORY COMMITTEE FOR AERONAUTICS

RESEARCH MEMORANDUM

A SEMIGRAPHICAL METHOD FOR THE DETERMINATION OF THE ROLLING CHARACTERISTICS OF ROLLERON-EQUIPPED MISSILES

By Martin L. Nason

SUMMARY

A semigraphical analysis method has been devised to evaluate the effectiveness and dynamic stability of rolleron roll-rate dampers on missile configurations. The necessary charts, equations, and the analysis procedure have been presented. The greatest utility of these charts and of the method outlined is that, once a point on the charts has been established at a given flight condition, if the response is not acceptable then the necessary modifications to the parameters of the system are readily seen.

INTRODUCTION

Present-day missile configurations possess, in general, inherently low aerodynamic roll damping. This is a consequence of the predominance of low-aspect-ratio lifting surfaces, which are the primary source of aerodynamic roll damping on conventional missiles. Rolling moments caused by lifting surface misalinements as well as combined angles of attack and sideslip may be of appreciable magnitude, and, as a result, rolling velocities are often produced which are well above the maximum allowed by the missile guidance system. A common solution of this problem is to install in the missile a servomechanism system which senses roll rate and furnishes a signal to a servo which actuates an aileron in the proper manner to oppose the rolling motion. The components for this roll control system, unfortunately, require missile space and the unavoidable complexity of the rate gyro tends to reduce the overall reliability of the missile. An urgent need therefore exists for a purely aeromechanical roll damper utilizing no internal missile components.

In reference 1 an analysis and flight test of a mechanically simple roll damper is described. In order to explore the applicability of this

type of damper on other missile configurations, an extension and generalization of the analysis reported therein has been performed and is reported in this paper. Design charts from which the static and dynamic characteristics of the roll mode can be obtained are presented. No attempt has been made, herein, to analyze any one particular missile completely with respect to the relative importance of the airframe and control surface parameters involved. Rather, equations and charts are presented to facilitate and expedite the analysis, design, and installation of this type of roll damper on missiles in general. An example of the use of these design charts is included for one particular missile configuration.

SYMBOLS

A normalized coefficient of characteristic equation

B normalized coefficient of characteristic equation

b wing span, ft

C_h hinge-moment coefficient, $\frac{H}{qSb}$

$C_{h_\delta} = \frac{\partial C_h}{\partial \delta}$, per radian

$C_{h_{\dot{\delta}}} = \frac{\partial C_h}{\partial \frac{b\dot{\delta}}{2V}}$, per radian

C_l rolling-moment coefficient, $\frac{L}{qSb}$

C_{l_o} external rolling-moment coefficient

$C_{l_p} = \frac{\partial C_l}{\partial \frac{b\dot{\phi}}{2V}}$, per radian

$C_{l_\delta} = \frac{\partial C_l}{\partial \delta}$, per radian (applies to only one surface)

D nondimensional differential operator, $T\frac{d}{dt}$

F conversion factor

H hinge moment, ft-lb

I_G moment of inertia of gyro wheel about spin axis, slug-ft^2

I_p rolleron product of inertia, $\int_{\text{Control surface}} uv\,dm$, slug-ft^2

I_R moment of inertia of rolleron about hinge line, slug-ft^2

$I_{R_c} = I_R - n\frac{I_p^2}{I_X}$

I_X moment of inertia of missile about longitudinal axis, slug-ft^2

$\bar{i},\bar{j},\bar{k}$ unit vectors along the X-, Y-, and Z-axes, respectively (orthogonal vectors)

$k = I_R/I_{R_c}$

L rolling moment, ft-lb

M Mach number

m mass of rolleron, slugs

m_G mass of rolleron gyro wheel, slugs

n number of rollerons on missile

p differential operator, $\frac{d}{dt}$

q dynamic pressure, lb/sq ft

S total wing area in one plane, sq ft

s nondimensional differential operator, D/F

T time constant, $\frac{b}{V\sqrt{\sigma}}$, sec

u	distance measured from hinge line, ft
V	missile velocity, ft/sec
v	distance measured from longitudinal axis, ft
α_1,α_2	real roots of normalized characteristic equation
δ	control-surface angular deflection, radians
ζ	damping ratio of a quadratic factor
ρ	density of air, slugs/cu ft
ρ_o	sea-level air density, 0.002378 slug/cu ft
σ	air-density ratio, ρ/ρ_o
ϕ	missile roll angle, radians
τ_1,τ_2,τ_3	real roots of characteristic equation
ω'	nondimensional undamped natural frequency
ω_G	gyro-wheel angular velocity, radians/sec
ω_n	undamped natural frequency, radians/sec

Subscript:

SS	steady state

ROLLERON OPERATING PRINCIPLE

A diagrammatic sketch of the roll damper is shown in figure 1. The roll control surface is mounted on the wing tip and is hinged forward of the center of pressure to produce stable hinge-moment characteristics. A gyro wheel is enclosed within the control surface with its spin axis perpendicular to the plane of the control surface. Because of the angular velocity of the gyro wheel ω_G, precessional hinge moments will act on the control surface whenever the missile has a rolling velocity $\dot{\phi}$. For the arrangement sketched, the control-surface deflection, caused by the precessional hinge moment, generates an aerodynamic rolling moment on the missile opposite to the assumed direction of roll velocity. Thus,

resistance to rolling is generated and the roll damping of the missile has been increased. The adopted name for this roll damper is rolleron and will be used for the remainder of this report.

Only one rolleron is indicated in the sketch; however, from longitudinal coupling considerations pairs of symmetrically located rollerons may be necessary or perhaps desirable. It should be noted that this roll-control system does not provide a roll-position reference and will not give zero roll rate in the presence of any sustained moment about the longitudinal axis of the missile.

ANALYSIS

In the analysis to follow, linerarized equations are used throughout. Only the rolling motion is considered. This simplification is justified on the basis of the results reported in reference 1 in which a similar analysis was performed on a specific missile and roll stability was predicted and experimentally confirmed in the presence of pitching and yawing oscillations.

Equations of Motion

If no pitching or yawing motion of the missile is assumed and if n rollerons are mounted on the missile, the following equations are valid:

For the missile:

$$\frac{I_X}{qSb}\ddot{\phi} - C_{l_p}\left(\frac{b}{2V}\right)\dot{\phi} - n\frac{I_p}{qSb}\ddot{\delta} - n\frac{\left(I_G\omega_G\right)}{qSb}\dot{\delta} - n\,C_{l_\delta}\delta = C_{l_o} \tag{1}$$

For the rolleron:

$$-\frac{I_p}{qSb}\ddot{\phi} + \frac{\left(I_G\omega_G\right)}{qSb}\dot{\phi} + \frac{I_R}{qSb}\ddot{\delta} - C_{h_\delta}\left(\frac{b}{2V}\right)\dot{\delta} - C_{h_\delta}\delta = 0 \tag{2}$$

Equation (1) is obtained by summing moments about the longitudinal axis of the missile and contains, in addition to the conventional aerodynamic and inertia terms $\left(C_{l_p},\ C_{l_\delta}, \text{ and } I_X\right)$, the rolleron product of inertia I_p and the rolleron wheel gyroscopic term $I_G\omega_G$. Equation (2) is derived by summing moments about the rolleron hinge line and applies to any one of the n rollerons since each is undergoing a similar motion. The second equation contains the conventional aerodynamic

hinge-moment parameter C_{h_δ} and inertia parameter I_R. The three remaining terms $I_G\omega_G$, I_p, and $C_{h_{\dot{\delta}}}$ are the rolleron gyroscopic term, the rolleron product of inertia, and the control-surface damping parameter, respectively. (The derivation of the rolleron gyroscopic hinge moments is presented in appendix A.)

The equations of motion can be placed into a more useful form by nondimensionalizing the time scale and by considering the rolleron product of inertia as a modification of the rolleron moment of inertia. See appendix B. Thus, by letting the differential operator $D = T\frac{d}{dt}$ where $T = \frac{b}{V\sqrt{\sigma}}$ and also by letting $k = \frac{I_R}{I_{R_c}}$ where I_{R_c} is the modified rolleron moment of inertia, the equations of motion become

$$\left(D - l_p\right)D\phi - \left(\frac{I_p}{I_X}D^2 + l_\omega D + l_\delta\right)n\delta = f \tag{3}$$

$$\left(-h_u D + h_\omega\right)D\phi + \left(kD^2 - h_v D - h_\delta\right)\delta = 0 \tag{4}$$

where

$$h_v = \frac{\sqrt{\sigma}}{2}\left(\frac{\rho_o S b^3}{2I_{R_c}}\right)C_{h_{\dot{\delta}}} \tag{5}$$

$$h_\delta = \left(\frac{\rho_o S b^3}{2I_{R_c}}\right)C_{h_\delta} \tag{6}$$

$$h_\omega = \frac{I_G}{I_{R_c}}\frac{b\omega_G}{V\sqrt{\sigma}} \tag{7}$$

$$h_u = \frac{I_p}{I_{R_c}} \tag{8}$$

$$l_p = \frac{\sqrt{\sigma}}{2}\left(\frac{\rho_o S b^3}{2I_X}\right)C_{l_p} \tag{9}$$

$$l_\delta = \left(\frac{\rho_o S b^3}{2I_x}\right) C_{l_\delta} \tag{10}$$

$$l_\omega = \frac{I_G}{I_X} \frac{b\omega_G}{V\sqrt{\sigma}} \tag{11}$$

$$f = \left(\frac{\rho_o S b^3}{2I_X}\right) C_{l_o} \tag{12}$$

and

$$I_{R_c} = I_R - n \frac{I_p^2}{I_X} \tag{13}$$

The ratio $\frac{T}{b}$ is plotted in figure 2 as a function of Mach number and altitude and $\sqrt{\sigma}$ is plotted in figure 3 as a function of altitude.

Dynamic Characteristics

The oscillatory characteristics of the rolleron system are determined by examination of the roots of the characteristic equation defined by the simultaneous equations (3) and (4). The characteristic equation is given as follows:

$$D^3 + a_1 D^2 + a_2 D + a_3 = 0 \tag{14}$$

Equation (14) can be reduced to the form

$$s^3 + As^2 + Bs + 1 = 0 \tag{15}$$

by replacing the differential operator D by Fs where

$$F = \sqrt[3]{a_3} = \sqrt[3]{h_\delta l_p + n h_\omega l_\delta} \tag{16}$$

$$A = \frac{a_1}{F} = \frac{-h_v - k l_p}{F} \tag{17}$$

$$B = \frac{a_2}{F^2} = \frac{h_v l_p - h_\delta + n h_\omega l_\omega - n h_u l_\delta}{F^2} \tag{18}$$

In order to show the relationship between the normalized coefficients A and B and the system aerodynamic and inertia parameters defined by equations (5) to (11), two series of charts were prepared and are presented in figures 4 and 5, respectively. The procedures for reading these charts are similar. These charts allow equations (17) and (18) to be visualized graphically and reveal the relative contribution of the various parameters of the system on the normalized coefficients A and B.

The procedure for reading the A coefficient chart (see sketch) is as follows:

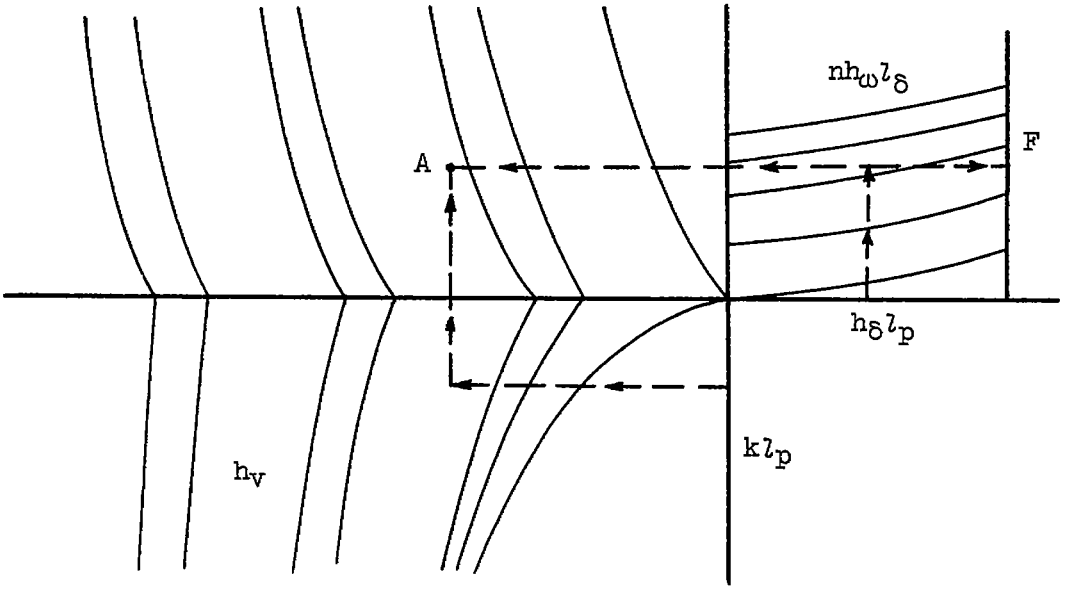

When the four parameters h_v, kl_p, $h_\delta l_p$, and $nh_\omega l_\delta$ have been calculated, then the dashed lines indicated are constructed on the plots and their intersection determines the value of A. By following the dashed line horizontally to the right from the correct $nh_\omega l_\delta$ contour line, the value of F is also given; F is used later as a conversion factor to obtain the correct time scale.

The roots of equation (15) that are of interest fall into two groups depending on the values of A and B. These are as follows:

Group I (one real and two complex roots ($\zeta < 1$)):

$$\left[s + \frac{1}{(\omega')^2}\right]\left[s^2 + 2\zeta\omega' s + (\omega')^2\right] = 0 \qquad (19)$$

Group II (three real roots):

$$\left(s + \frac{1}{\alpha_1\alpha_2}\right)\left(s + \alpha_1\right)\left(s + \alpha_2\right) = 0 \tag{20}$$

By setting equations (19) and (20) equal to equation (15) and equating corresponding coefficients, the following equations can be obtained:

For group I ($0 < \zeta < 1$),

$$A = 2\zeta\omega' + \frac{1}{(\omega')^2} \tag{21}$$

$$B = (\omega')^2 + \frac{2\zeta}{\omega'} \tag{22}$$

For group II,

$$A = \left(\alpha_1 + \alpha_2\right) + \frac{1}{\alpha_1\alpha_2} \tag{23}$$

$$B = \alpha_1\alpha_2 + \frac{\alpha_1 + \alpha_2}{\alpha_1\alpha_2} \tag{24}$$

The regions in the A-B plane where the roots represented by groups I and II exist are sketched in figure 6 for a limited range of A and B. Only the first quadrant where A and B are both positive is shown, since when either A or B is negative a dynamic instability exists and this region is of no interest. The oscillatory stability boundary is located where the product of A and B is equal to unity or where the damping ratio ζ is equal to zero. The boundary separating the regions where roots defined by groups I and II exist is obtained by setting ζ equal to unity in equations (21) and (22). This boundary is fan-shaped and is symmetrically located in the positive A-B plane. The point $A = B = 3$ corresponds to the situation where the normalized cubic equation possesses three real and equal roots.

This method of solving the cubic equation was reported in reference 2 and the treatment here is similar except for the description of the region in the A-B plane occupied by roots corresponding to group II. The ambiguity encountered in reference 2 is eliminated by utilizing equation (20) rather than equation (19) to represent the roots for group II.

Plots of A against B for constant values of ζ, ω', α_1, and α_2 can be constructed using equations (21) to (24). These charts are shown in figures 7 and 8 for $0 < A < 28$ and $0 < B < 202$ for groups I and II, respectively. For group II the α_1 and $\alpha_1\alpha_2$ contours were plotted

rather than the α_1 and α_2 contours because the α_1^2 and $\alpha_1\alpha_2$ contours intersect one another at nearly right angles and better definition of the region is achieved.

Static Characteristics

Solving equations (3) and (4) for the steady-state values of $D\phi$ and δ to a constant input f leads to

$$-\left(\frac{f}{D\phi}\right)_{ss} = \frac{h_\delta l_p + n h_\omega l_\delta}{h_\delta} \tag{25}$$

or

$$-\left(\frac{f}{D\phi}\right)_{ss} = l_p + \frac{n h_\omega l_\delta}{h_\delta} \tag{26}$$

and

$$-\left(\frac{\delta}{f}\right)_{ss} = \frac{h_\omega}{h_\delta l_p + n h_\omega l_\delta} \tag{27}$$

By inspecting equation (26), the additional increase in missile steady-state roll damping contributed by the rollerons becomes apparent. The inherent aerodynamic roll damping of the missile is proportional to l_p and the rolleron contribution is proportional to $\frac{n h_\omega l_\delta}{h_\delta}$. When the rolleron wheel is not rotating, h_ω is equal to zero and no additional damping is present.

Equations (25) and (27) are solved graphically in figure 9. The procedure for finding $-\left(\frac{f}{D\phi}\right)_{ss}$ and $-\left(\frac{\delta}{f}\right)_{ss}$ is shown by the dashed lines in the following sketch of the rolleron steady-state chart:

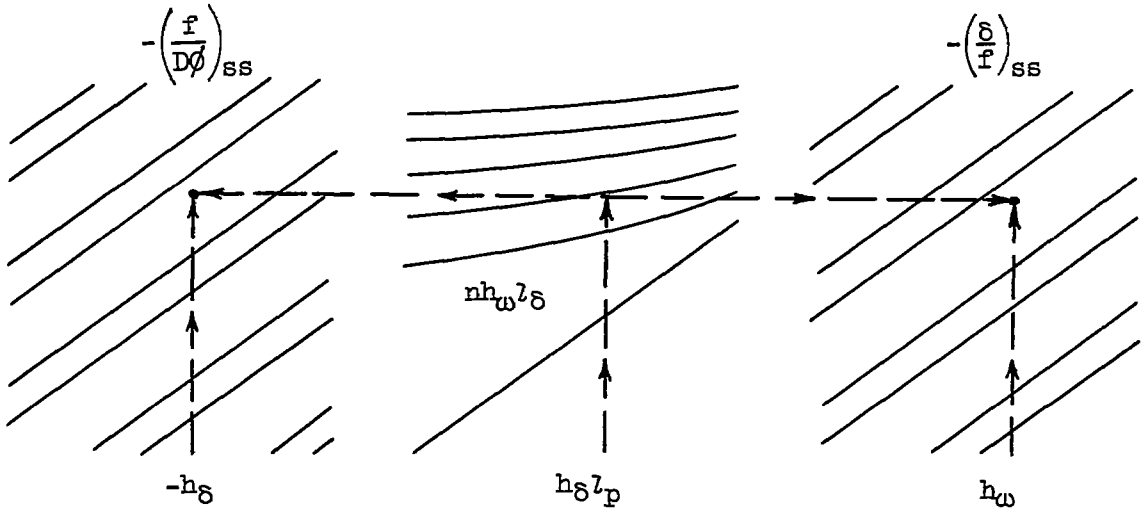

Conversion to Real Time

Because of the nondimensionalizing techniques employed, the dynamic and static characteristics obtained from the charts are in a dimensionless time scale. Conversion to real time may be accomplished by multiplication of the time constants and natural frequencies involved by the appropriate factors.

Dynamic characteristics.- The system characteristic equation with the differential operator $p = \frac{d}{dt}$ is as follows:

For group I,

$$\left(p + \tau_1\right)\left(p^2 + 2\zeta\omega_n p + \omega_n{}^2\right) = 0 \tag{28}$$

where

$$\tau_1 = \left(\frac{F}{T}\right)\frac{1}{(\omega')^2}, \text{ sec}^{-1} \tag{29}$$

$$\omega_n = \left(\frac{F}{T}\right)\omega', \text{ radians/sec} \tag{30}$$

For group II,

$$\left(p + \tau_1\right)\left(p + \tau_2\right)\left(p + \tau_3\right) = 0 \tag{31}$$

where

$$\tau_1 = \left(\frac{F}{T}\right)\alpha_1, \ \text{sec}^{-1} \tag{32}$$

$$\tau_2 = \left(\frac{F}{T}\right)\alpha_2, \ \text{sec}^{-1} \tag{33}$$

$$\tau_3 = \left(\frac{F}{T}\right)\frac{1}{\alpha_1\alpha_2}, \ \text{sec}^{-1} \tag{34}$$

Since ζ is a nondimensional ratio and does not involve time, no time conversion is required.

Static characteristics.- The steady-state equations are obtained by multiplying equations (25) and (27) by the correct conversion factors as follows:

$$-\left(\frac{C_{l_o}}{\frac{b\dot{\phi}}{2V}}\right)_{ss} = \frac{2}{\sqrt{\sigma}}\left(\frac{2I_x}{\rho_o Sb^3}\right)\left[-\left(\frac{f}{D\phi}\right)_{ss}\right] \tag{35}$$

and

$$-\left(\frac{\delta}{C_{l_o}}\right)_{ss} = \left(\frac{\rho_o Sb^3}{2I_x}\right)\left[-\left(\frac{\delta}{f}\right)_{ss}\right] \tag{36}$$

RESULTS AND DISCUSSION

From the results of the preceding analysis section, a semigraphical procedure can be formulated which will reduce the analysis time required to study the feasibility of the installation of rollerons on a specific missile design. This graphical method to be outlined furnishes a considerable amount of information concerning the dynamic stability and the roll damping contribution of a given missile-rolleron configuration.

The following steps are required for this method:

Step 1: Tabulate the missile and rolleron geometrical and inertia characteristics S, b, I_X, I_G, I_{R_c}, k, and Ip.

Step 2: Decide on the Mach number and altitude conditions to be studied and then determine T and $\sqrt{\sigma}$ from figures 2 and 3.

Step 3: Estimate the aerodynamic coefficients C_{h_δ}, C_{l_p}, C_{l_δ}, and C_{h_δ} and the rolleron gyro-wheel angular velocity ω_G.

Step 4: Compute h_v, h_δ, h_ω, h_u, l_p, l_δ, and l_ω by using equations (5) to (11).

Step 5: From figures 4 and 5 determine the values of A, B, and F. Check the product of A and B and if the value is less than unity the system will require modification.

Step 6: From either figure 7 or 8 (depending on the values of A and B), determine the dimensionless factors of the normalized characteristic equation.

Step 7: Convert the dimensionless factors to real time using equations (29) and (30) or equations (32), (33), and (34).

Step 8: From figure 9, determine the static characteristics $-\left(\frac{f}{D\phi}\right)_{ss}$ and $-\left(\frac{\delta}{f}\right)_{ss}$.

Step 9: Convert the static characteristics to a more useful form by use of equations (35) and (36).

The foregoing procedure is quite flexible in that the effect of individual parameter changes does not require a reiteration of all nine steps. This feature will be brought out in the following example.

Example

In order to illustrate the use of the charts, a typical problem will be solved. The configuration reported in reference 1 is chosen as the missile to be analyzed. The steps in the design procedure give the following results when four rollerons are installed and the control surface damping is assumed to be equal to zero:

Step 1:

$$S = 2.73 \text{ sq ft}$$

$$b = 1.73 \text{ ft}$$

$$I_X = 0.299 \text{ slug-ft}^2$$

Step 1 - Continued:

$$I_G = 0.000201 \text{ slug-ft}^2$$

$$I_{R_c} = 0.000581 \text{ slug-ft}^2$$

$$k = 1.21$$

$$I_p = 0.0031 \text{ slug-ft}^2$$

Step 2:

$$M = 2.0$$

$$\text{Altitude} = 20{,}000 \text{ ft}$$

$$T = 0.00115 \text{ sec},$$

$$\sqrt{\sigma} = 0.73$$

Step 3:

$$C_{h_\delta} = -0.00324, \text{ per radian}$$

$$C_{l_p} = -0.282, \text{ per radian}$$

$$C_{l_\delta} = 0.0204, \text{ per radian}$$

$$C_{h_{\dot{\delta}}} = 0$$

$$\omega_G = 400 \text{ radians/sec}$$

Step 4:

$h_v = 0$	$-kl_p = 0.00695$
$h_\delta = -0.0942$	$h_\delta l_p = 0.000541$
$h_\omega = 0.159$	$nh_\omega l_\delta = 0.000719$
$h_u = 5.34$	$-h_\delta - nh_u l_\delta = 0.0701$

Step 4 - Continued:

$l_p = -0.00574$ $\qquad h_v l_p + n h_\omega l_\omega = 0.000196$

$l_\delta = 0.00113$

$l_\omega = 0.000308$

Step 5:

$A = 0.0643$ $\qquad B = 8.1$
$AB = 0.521$ $\qquad F = 0.108$

Note here that the product of A and B is less than unity which corresponds to the region in the A-B plane where a dynamic instability exists. Therefore, there is no reason to proceed any further without modifying the rolleron system. A possible modification to the system would be to introduce control-surface damping about the rolleron hinge line. Repeating step 5 for $h_v = -0.5$ gives

Step 5:

$A = 4.69$ $\qquad B = 8.35$

$AB = 39.2$ $\qquad F = 0.108$

Step 6:

$\zeta = 0.82$ $\qquad \omega' = 2.77$

Step 7:

$\tau_1 = 12.2 \text{ sec}^{-1}$

$\zeta = 0.82$

$\omega_n = 256$ radians/sec

Step 8:

$$\left(\frac{f}{D\phi}\right)_{ss} = 0.0134$$

$$\left(\frac{\delta}{f}\right)_{ss} = -126.2$$

Step 9:

$$\left(\frac{C_{l_o}}{\frac{b\dot{\phi}}{2V}}\right)_{ss} = 0.653 \text{ per radian}$$

$$\left(\frac{\delta}{C_{l_o}}\right)_{ss} = -5.16 \text{ radians}$$

After experience has been acquired with the charts and with the missile being investigated, systematic system variation can be tried and an acceptable design fix established.

The greatest utility of these charts and of the method outlined is that, once a point in the A-B plane has been established at a given flight condition, if the response is not acceptable then the change in either A or B or both which will yield an acceptable response is readily seen. Then, it is only necessary to investigate the A and B coefficient plots to determine which parameters of the system must be modified to move the point in the A-B plane to the desired position. Depending upon the configuration under investigation, different parameters will probably be critical. However, from a study of two missile configurations, it was found necessary in both cases to increase A by increasing the system parameter h_V to a degree where the contribution of l_p to the A coefficient was negligible.

CONCLUDING REMARKS

A semigraphical analysis method has been devised to evaluate the effectiveness and dynamic stability of rolleron roll-rate dampers on missile configurations. The necessary charts, equations, and the analysis procedure have been presented. The greatest utility of these charts and of the method outlined is that, once a point on the charts has been established at a given flight condition, if the response is not acceptable then the necessary modifications to the system parameters are readily seen.

Langley Aeronautical Laboratory,
National Advisory Committee for Aeronautics,
Langley Field, Va., August 23, 1956.

APPENDIX A

ROLLERON GYROSCOPIC HINGE MOMENTS

The vector expression relating the gyroscopic hinge moment $\bar{H}_G$ to the missile angular velocity $\bar{\omega}_m$ and the rolleron gyro-wheel angular velocity $\bar{\omega}_G$ is (see ref. 3) as follows:

$$-\bar{H}_G = I_G\bar{\omega}_G \times \bar{\omega}_m + J\dot{\bar{\omega}}_m \tag{A1}$$

where J is the moment of inertia of the gyro wheel about an axis normal to the spin axis and I_G is the moment of inertia of the gyro wheel about the spin axis. The angular velocity of the missile $\bar{\omega}_m$ is represented by a vector having three component about the X-, Y-, and Z-axes, respectively. Thus,

$$\bar{\omega}_m = \dot{\phi}\bar{i} + \dot{\theta}\bar{j} + \dot{\psi}\bar{k} \tag{A2}$$

The vector expression for the gyro-wheel angular velocity is readily found once the control-surface angular deflection is known and the geometric position of the wheel with respect to the axis system is specified. Two cases are considered here: (1) rollerons coincident with the X-Y and X-Z planes and (2) rollerons in a 45° plane between the X-Y and X-Z planes. These two cases are sketched for four rollerons - designated n = 0, 1, 2, and 3:

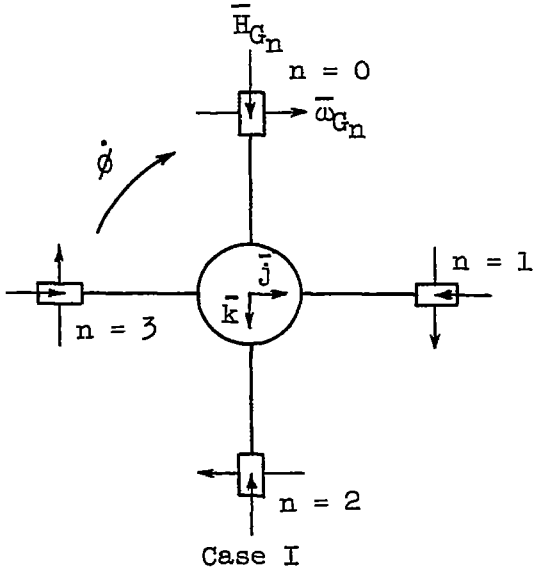

Case I

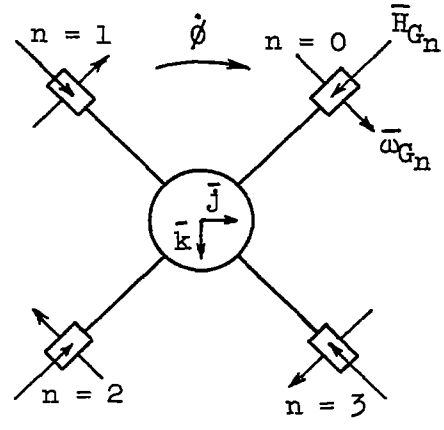

Case II

Case I.- It can be shown that the gyro-wheel angular velocity vector $\bar{\omega}_G$ is given by the following expression:

$$\bar{\omega}_{G_n} = \left|\bar{\omega}_{G_n}\right|\left(-\sin\delta_R\bar{i} + \cos\frac{n\pi}{2}\cos\delta_R\bar{j} + \sin\frac{n\pi}{2}\cos\delta_R\bar{k}\right) \tag{A3}$$

where $n = 0, 1, 2,$ and 3. Substituting equations (A2) and (A3) into equation (A1) leads to the following equation:

$$-\bar{H}_{G_n} = I_G\left|\bar{\omega}_{G_n}\right|\left[\left(-\sin\frac{n\pi}{2}\cos\delta_R\dot{\theta} + \cos\frac{n\pi}{2}\cos\delta_R\dot{\psi}\right)\bar{i} + \left(\sin\frac{n\pi}{2}\cos\delta_R\dot{\phi} + \sin\delta_R\dot{\psi}\right)\bar{j} + \left(-\cos\frac{n\pi}{2}\cos\delta_R\dot{\phi} - \sin\delta_R\dot{\theta}\right)\bar{k}\right] + J\ddot{\phi}\bar{i} + J\ddot{\theta}\bar{j} + J\ddot{\psi}\bar{k} \tag{A4}$$

The vector $\bar{H}_{G_n}$ will not, in general, be coincident with the hinge line; however, the scalar expression for the hinge moment about the correct axis may be obtained by taking the dot product of $\bar{H}_{G_n}$ into a unit vector $\bar{U}_n$ along the hinge line:

$$-H_{G_n} = \bar{H}_{G_n} \cdot \bar{U}_n \tag{A5}$$

where

$$\bar{U}_n = -\sin\frac{n\pi}{2}\bar{j} + \cos\frac{n\pi}{2}\bar{k} \tag{A6}$$

Therefore,

$$-H_G = I_G\left|\bar{\omega}_{G_n}\right|\left[\left(\sin\frac{n\pi}{2}\cos\delta_R\dot{\phi} + \sin\delta_R\dot{\psi}\right)\left(-\sin\frac{n\pi}{2}\right) + \left(-\cos\frac{n\pi}{2}\cos\delta_R\dot{\phi} - \sin\delta_R\dot{\theta}\right)\left(\cos\frac{n\pi}{2}\right)\right] + J\dot{\theta}\ddot{\left(-\sin\frac{n\pi}{2}\right)} + J\dot{\psi}\ddot{\left(\cos\frac{n\pi}{2}\right)} \tag{A7}$$

Case II.- For case II, the gyro-wheel angular velocity vector becomes

$$\bar{\omega}_{G_n} = \left|\bar{\omega}_{G_n}\right|\left[-\sin\delta_R\bar{i} + \sin(2n+1)\frac{\pi}{4}\cos\delta_R\bar{j} + \cos(2n+1)\frac{\pi}{4}\cos\delta_R\bar{k}\right] \quad (A8)$$

Substituting equations (A2) and (A7) into equation (A1) yields

$$\begin{aligned}-\bar{H}_{G_n} = I_G\left|\bar{\omega}_{G_n}\right|\Bigg\{&\left[-\cos(2n+1)\frac{\pi}{4}\cos\delta_R\dot{\theta} + \sin(2n+1)\frac{\pi}{4}\cos\delta_R\dot{\psi}\right]\bar{i}\\ &\left[\cos(2n+1)\frac{\pi}{4}\cos\delta_R\dot{\phi} + \sin\delta_R\dot{\psi}\right]\bar{j} +\\ &\left[-\sin(2n+1)\frac{\pi}{4}\cos\delta_R\dot{\phi} - \sin\delta_R\dot{\theta}\right]\bar{k}\Bigg\} +\\ &J\ddot{\phi}\bar{j} + J\ddot{\theta}\bar{j} + J\ddot{\psi}\bar{k}\end{aligned} \quad (A9)$$

The dot product of $\bar{H}_{G_n}$ into a unit vector along the rolleron hinge line gives

$$-H_{G_n} = \bar{H}_{G_n}\cdot\left[-\cos(2n+1)\frac{\pi}{4}\bar{j} + \sin(2n+1)\frac{\pi}{4}\bar{k}\right] \quad (A10)$$

or

$$\begin{aligned}-H_{G_n} = I_G\left|\bar{\omega}_{G_n}\right|\Bigg\{&-\cos(2n+1)\frac{\pi}{4}\left[\cos(2n+1)\frac{\pi}{4}\cos\delta_R\dot{\phi} + \sin\delta_R\dot{\psi}\right] +\\ &\sin(2n+1)\frac{\pi}{4}\left[-\sin(2n+1)\frac{\pi}{4}\cos\delta_R\dot{\phi} - \sin\delta_R\dot{\theta}\right]\Bigg\} +\\ &J\ddot{\theta}\left[-\cos(2n+1)\frac{\pi}{4}\right] + J\ddot{\psi}\left[\sin(2n+1)\frac{\pi}{4}\right]\end{aligned} \quad (A11)$$

If it is assumed that the missile is undergoing no pitching or yawing motion and that the rolleron is not deflected, then $\delta_R = \ddot{\theta} = \dot{\theta} = \ddot{\psi} = \dot{\psi} = 0$ and the equation for the gyroscopic hinge moment for cases I and II become:

For case I,

$$-H_{G_n} = I_G\left|\bar{\omega}_{G_n}\right|\left(-\sin^2\frac{n\pi}{2}\dot{\phi} - \cos^2\frac{n\pi}{2}\dot{\phi}\right) \quad (A12)$$

For case II,

$$-H_{G_n} = I_G\left|\overline{\omega}_{G_n}\right|\left[-\cos^2(2n+1)\frac{\pi}{4}\dot{\phi} - \sin^2(2n+1)\frac{\pi}{4}\dot{\phi}\right] \qquad (A13)$$

Equations (A12) and (A13) reduce to

$$H_{G_n} = I_G\left|\overline{\omega}_{G_n}\right|\dot{\phi} \qquad (A14)$$

Equation (A14) implies, with the assumption of pure rolling motion and small control-surface deflections, that the gyroscopic hinge moment is independent of its orientation. Therefore, equation (A14) will apply to any one of the rollerons on the missile.

APPENDIX B

SIMPLIFICATION OF THE EQUATIONS OF MOTION FOR THE ROLLERON SYSTEM

The equations of motion (eqs. (1) and (2) in the text) of the missile and rolleron combination are as follows:

For the missile,

$$\frac{I_X}{qSb}\ddot{\phi} - C_{l_p}\left(\frac{b}{2V}\right)\dot{\phi} - n\frac{I_p}{qSb}\ddot{\delta} - n\frac{\left(I_G\omega_G\right)}{qSb}\dot{\delta} - nC_{l_\delta}\delta = C_{l_o} \tag{B1}$$

For the rolleron,

$$-\frac{I_p}{qSb}\ddot{\phi} + \frac{\left(I_G\omega_G\right)}{qSb}\dot{\phi} + \frac{I_R}{qSb}\ddot{\delta} - C_{h_{\dot{\delta}}}\left(\frac{b}{2V}\right)\dot{\delta} - C_{h_\delta}\delta = 0 \tag{B2}$$

By letting $D = T\frac{d}{dt}$ and multiplying equations (B1) and (B2) by $\frac{\rho_o Sb^3}{2I_X}$ and $\frac{\rho_o Sb^3}{2I_R}$, respectively, the following equations result:

$$\left(D - l_p\right)D\phi - \left(\frac{I_p}{I_X}D^2 + l_\omega D + l_\delta\right)n\delta = f \tag{B3}$$

$$\left(-\frac{I_p}{I_R}D + h_\omega'\right)D\phi + \left(D^2 - h_v'D - h_\delta'\right)\delta = 0 \tag{B4}$$

where l_p, l_δ, l_ω, and f are defined by equations (9) to (12) and where

$$h_v' = \frac{\sqrt{\sigma}}{2}\left(\frac{\rho_o Sb^3}{2I_R}\right)C_{h_{\dot{\delta}}}$$

$$h_\delta' = \left(\frac{\rho_o Sb^3}{2I_R}\right)C_{h_\delta}$$

$$h_\omega' = \frac{I_G}{I_R}\frac{b\omega_G}{V\sqrt{\sigma}}$$

[redacted]

The characteristic equation is thus:

$$a_0'D^3 + a_1'D^2 + a_2'D + a_3' = 0 \tag{B5}$$

where

$$a_0' = 1 - n\left(\frac{I_p}{I_X}\right)\left(\frac{I_p}{I_R}\right) \tag{B6}$$

$$a_1' = -h_v' - l_p \tag{B7}$$

$$a_2' = h_v' l_p - h_\delta' + nh_\omega' l_\omega - \frac{I_p}{I_R} l_\delta \tag{B8}$$

$$a_3' = h_\delta' l_p + nh_\omega' l_\delta \tag{B9}$$

It will now be proved that the a_0' coefficient can be normalized by modifying the moment of inertia I_R of the control surface without changing the values of the roots of equation (B5). If equation (B2) is multiplied by $\frac{\rho_o S b^3}{I_{R_c}}$, the equations of motion become

$$\left(D - l_p\right)D\phi - \left(\frac{I_p}{I_X} D^2 + l_\omega D + l_\delta\right)n\delta = f \tag{B10}$$

$$\left(-\frac{I_p}{I_{R_c}} D + h_\omega\right)D\phi + \left(\frac{I_R}{I_{R_c}} D^2 - h_v D - h_\delta\right)\delta = 0 \tag{B11}$$

Expanding the stability determinant by using the simultaneous equations (B10) and (B11) leads to the following results for the frequency equation:

$$a_0 D^3 + a_1 D^2 + a_2 D + a_3 = 0 \tag{B12}$$

where

$$a_0 = \frac{1}{I_{R_c}}\left(I_R - n\frac{I_p^2}{I_X}\right) \tag{B13}$$

$$a_1 = -h_v - \frac{I_R}{I_{R_c}} l_p \tag{B14}$$

$$a_2 = -h_\delta + h_v l_p - n\frac{I_p}{I_{R_c}} l_\delta + nh_\omega l_\omega \tag{B15}$$

$$a_3 = h_\delta l_p + nh_\omega l_\delta \tag{B16}$$

When I_{R_c} is defined as $I_R - n\frac{I_p^2}{I_X}$, it can easily be shown that

$$a_0 = a_0'\left(\frac{I_R}{I_{R_c}}\right) = 1 \tag{B17}$$

$$a_1 = a_1'\left(\frac{I_R}{I_{R_c}}\right) \tag{B18}$$

$$a_2 = a_2'\left(\frac{I_R}{I_{R_c}}\right) \tag{B19}$$

$$a_3 = a_3'\left(\frac{I_R}{I_{R_c}}\right) \tag{B20}$$

or

$$a_n = a_n'\left(\frac{I_R}{I_{R_c}}\right) \qquad (n = 0, 1, 2, 3) \tag{B21}$$

Since a rational, algebraic polynomial of the form given by equation (B5) can be multiplied by a constant without changing the values of the roots, equation (B21) implies that the roots of equations (B12) and (B5) are identical inasmuch as $\frac{I_R}{I_{R_c}}$ is a constant.

REFERENCES

1. Nason, Martin L., Brown, Clarence A., Jr., and Rock, Rupert S.: An Evaluation of a Rolleron-Roll-Rate Stabilization System for a Canard Missile Configuration at Mach Numbers From 0.9 to 2.3. NACA RM L55C22, 1955.

2. Evans, Leroy W.: Solution of the Cubic Equation and the Cubic Charts. M.I.T., 1943.

3. Joos, Georg: Theoretical Physics. Second ed., Hafner Pub. Co., Inc. (New York), 1950.

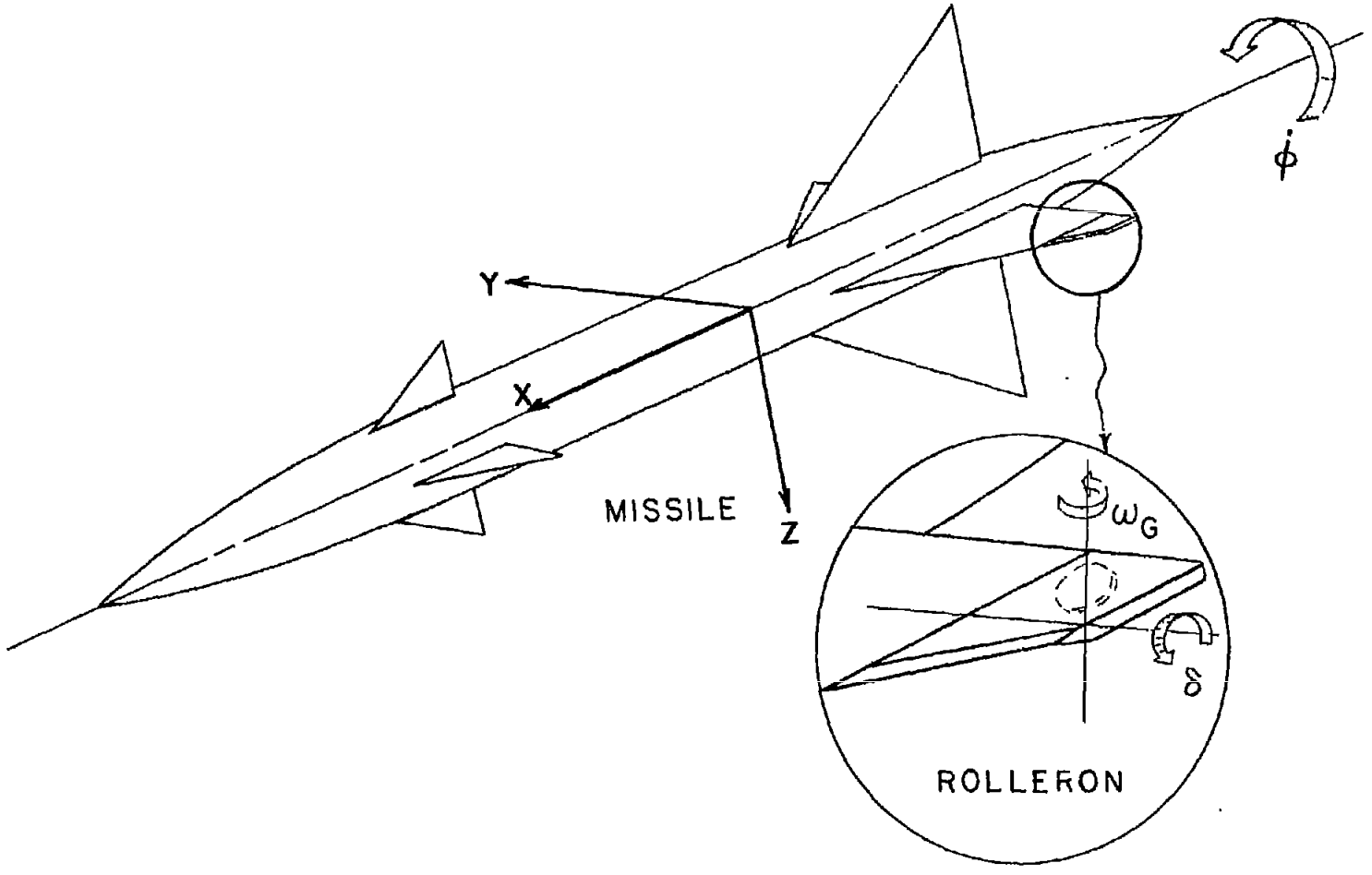

Figure 1.- Diagrammatic sketch of rolleron.

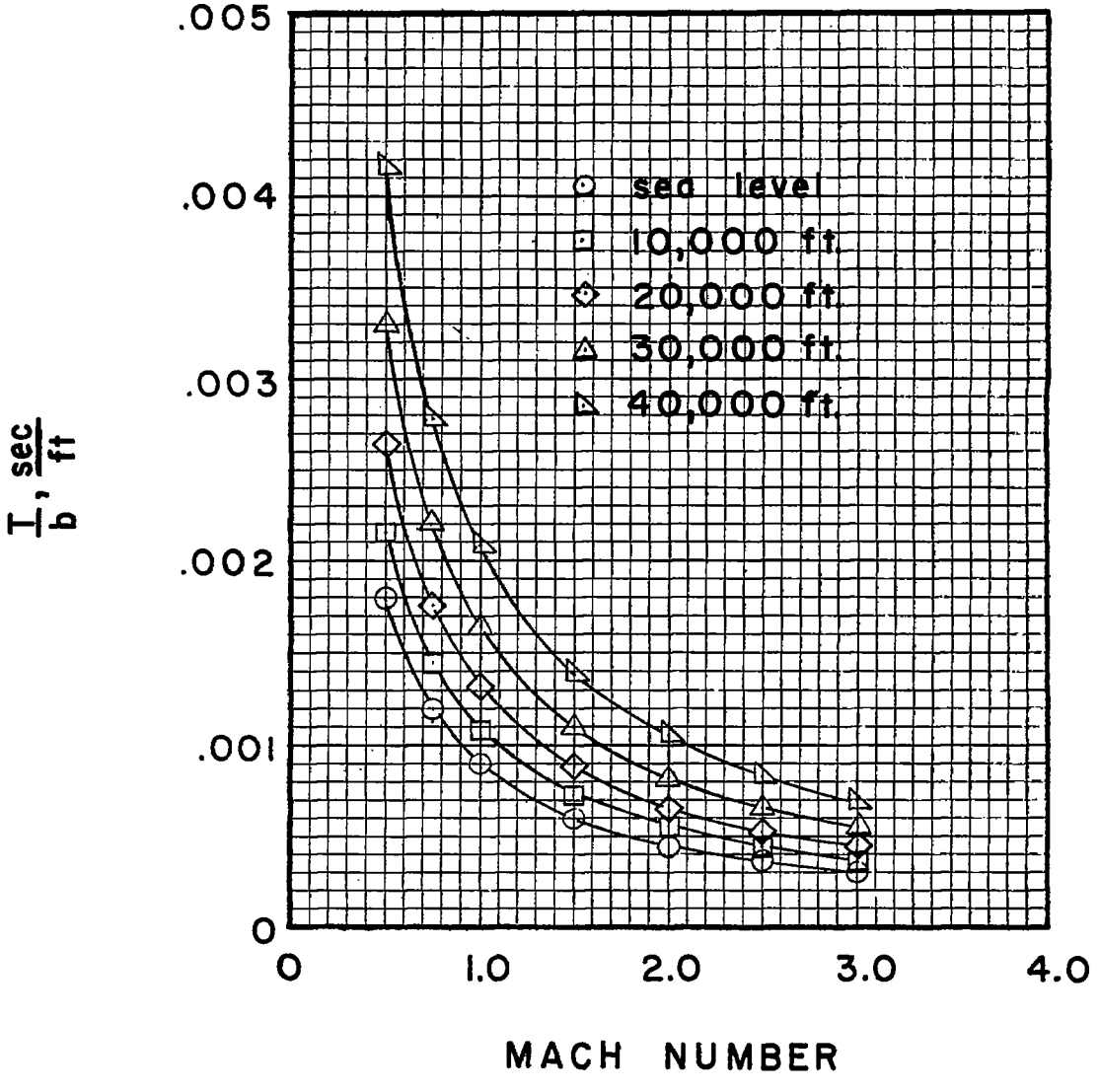

Figure 2.- Variation of T/b as a function of Mach number and altitude.

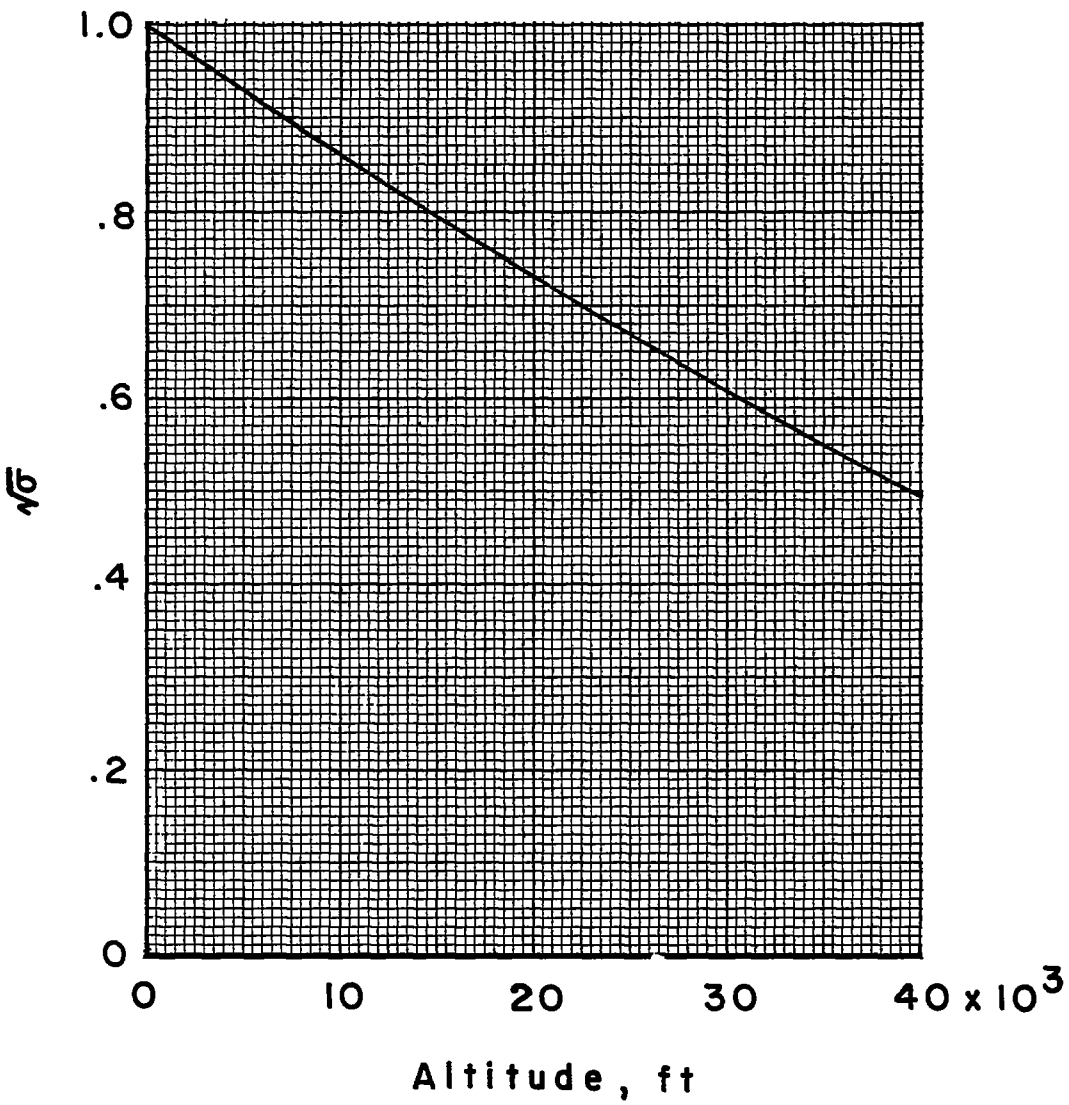

Figure 3.- Variation of $\sqrt{\sigma}$ as a function of altitude.

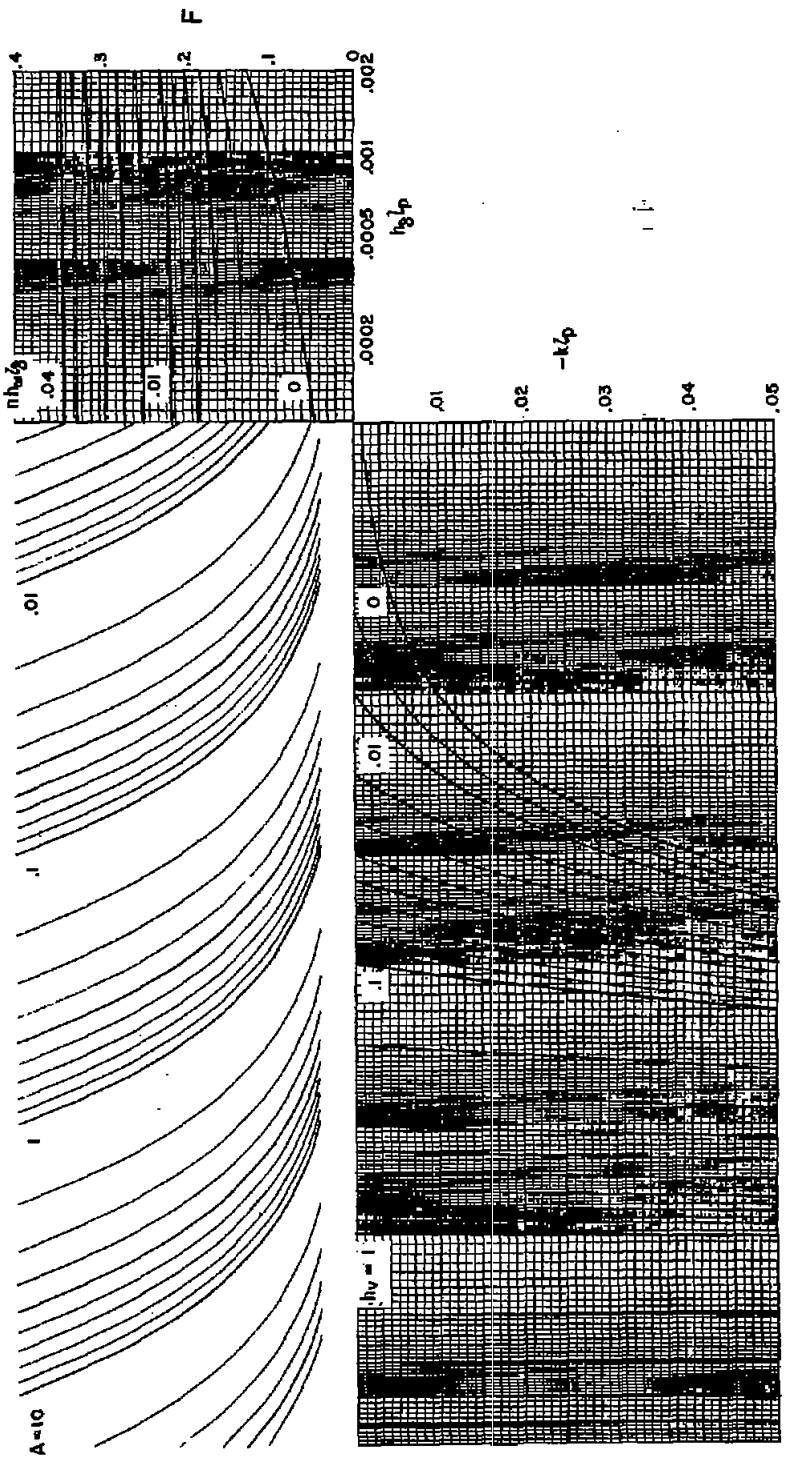

Figure 4.- A coefficient chart.

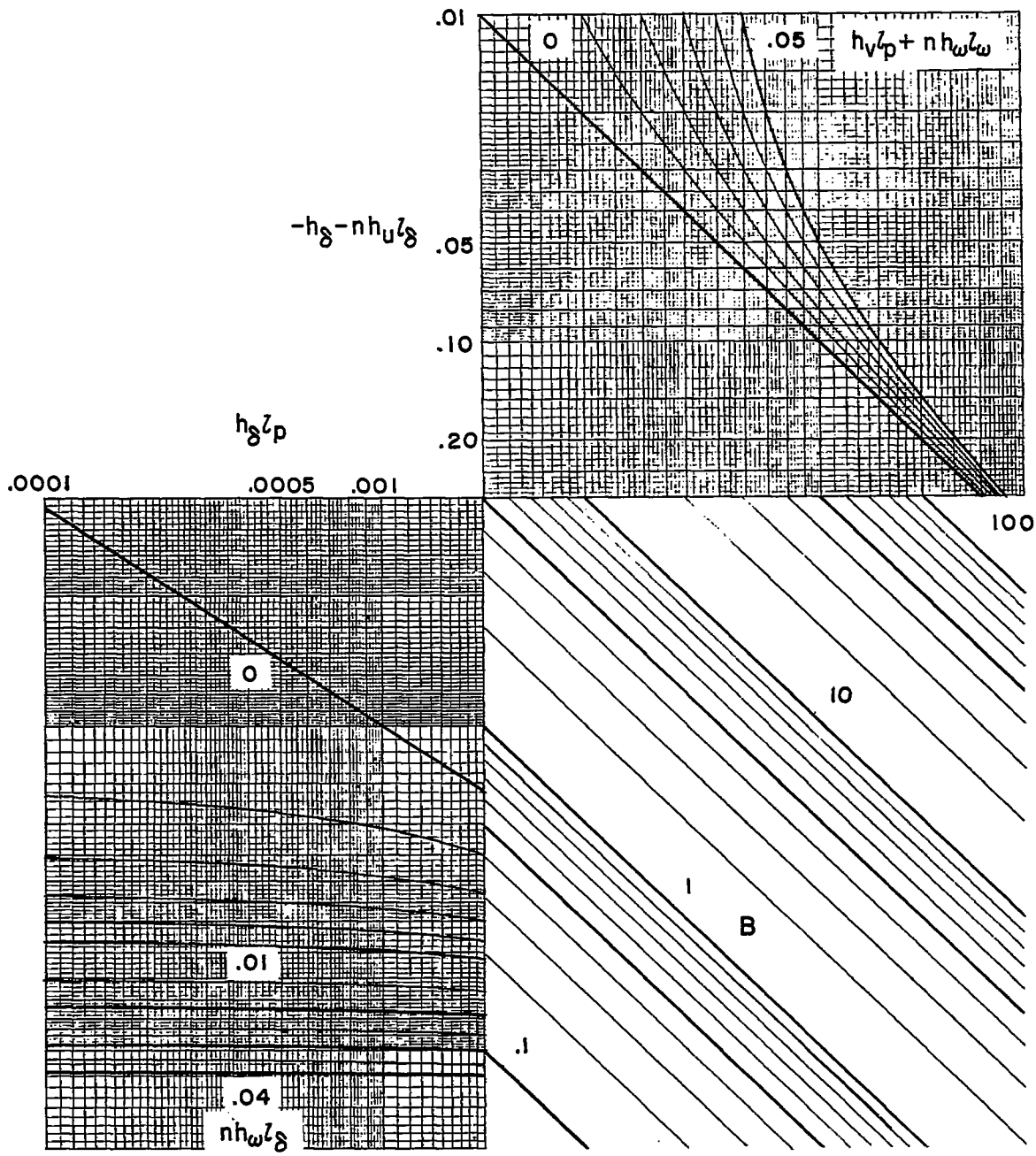

Figure 5.- B coefficient chart.

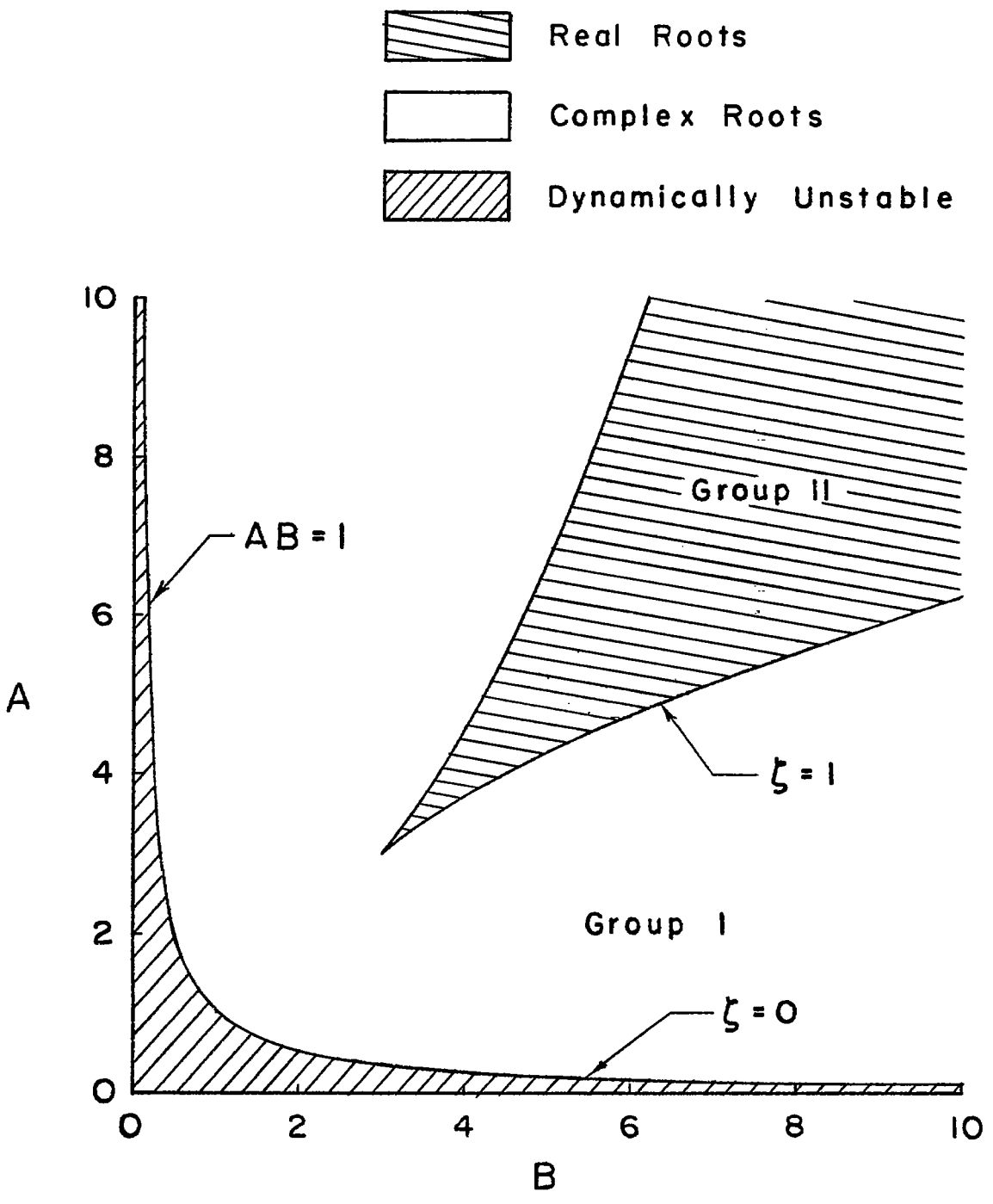

Figure 6.- Sketch of the A-B plane showing the root regions for the normalized cubic equation.

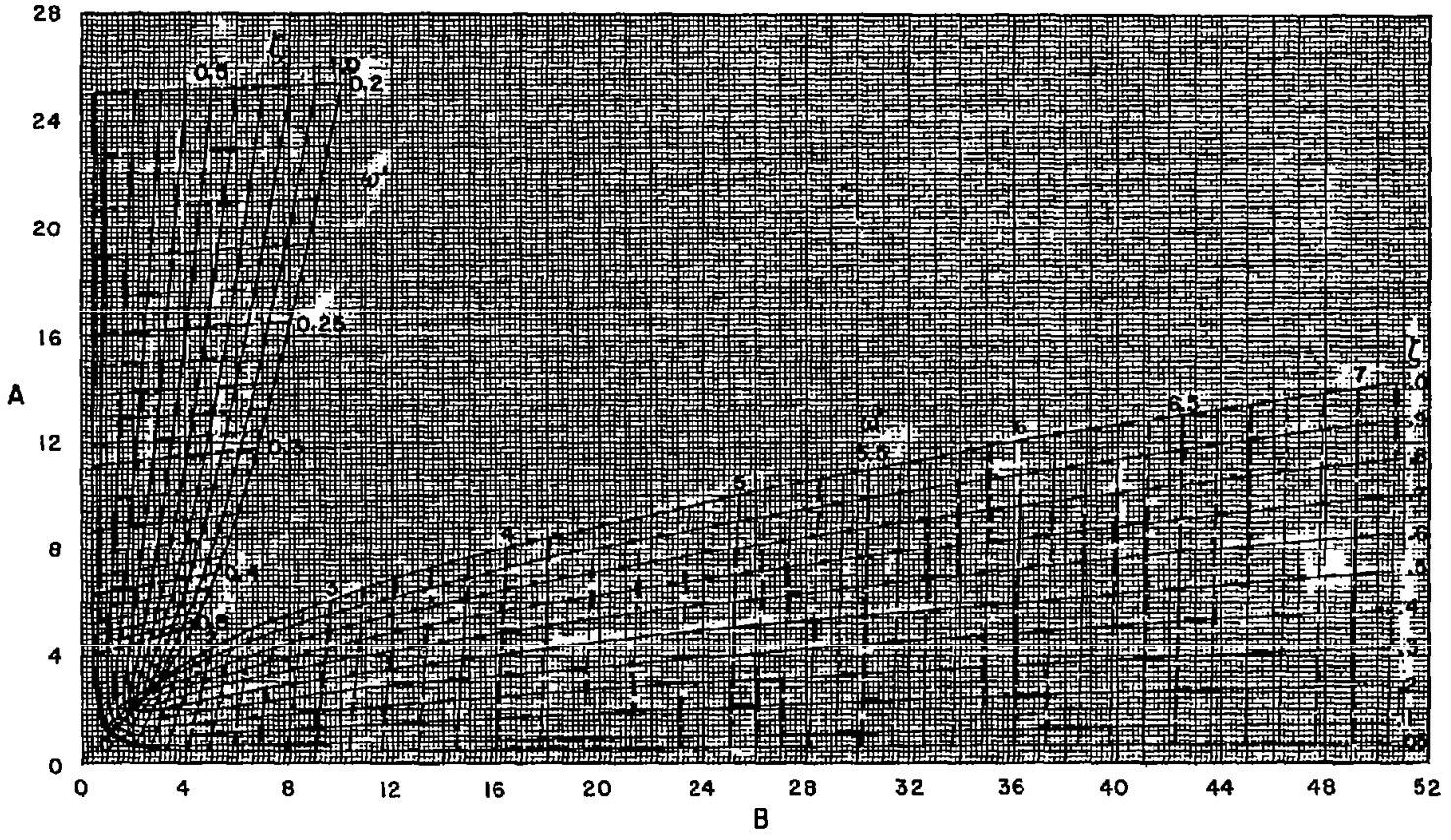

(a) $0 < B < 52$.

Figure 7.- Root charts for the normalized cubic equation when $0 < \zeta < 1$.

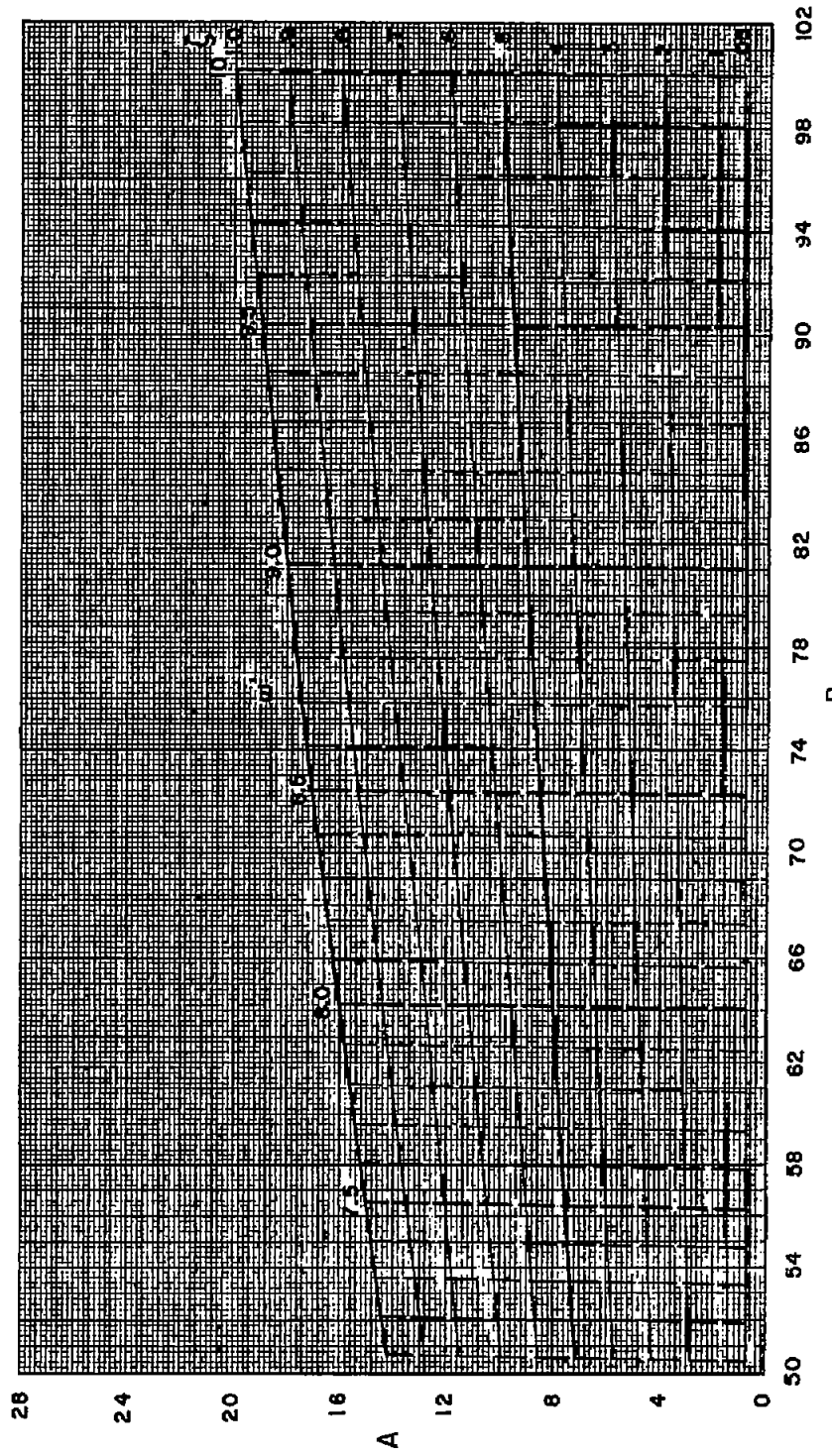

(b) $50 < B < 102$.

Figure 7.- Continued.

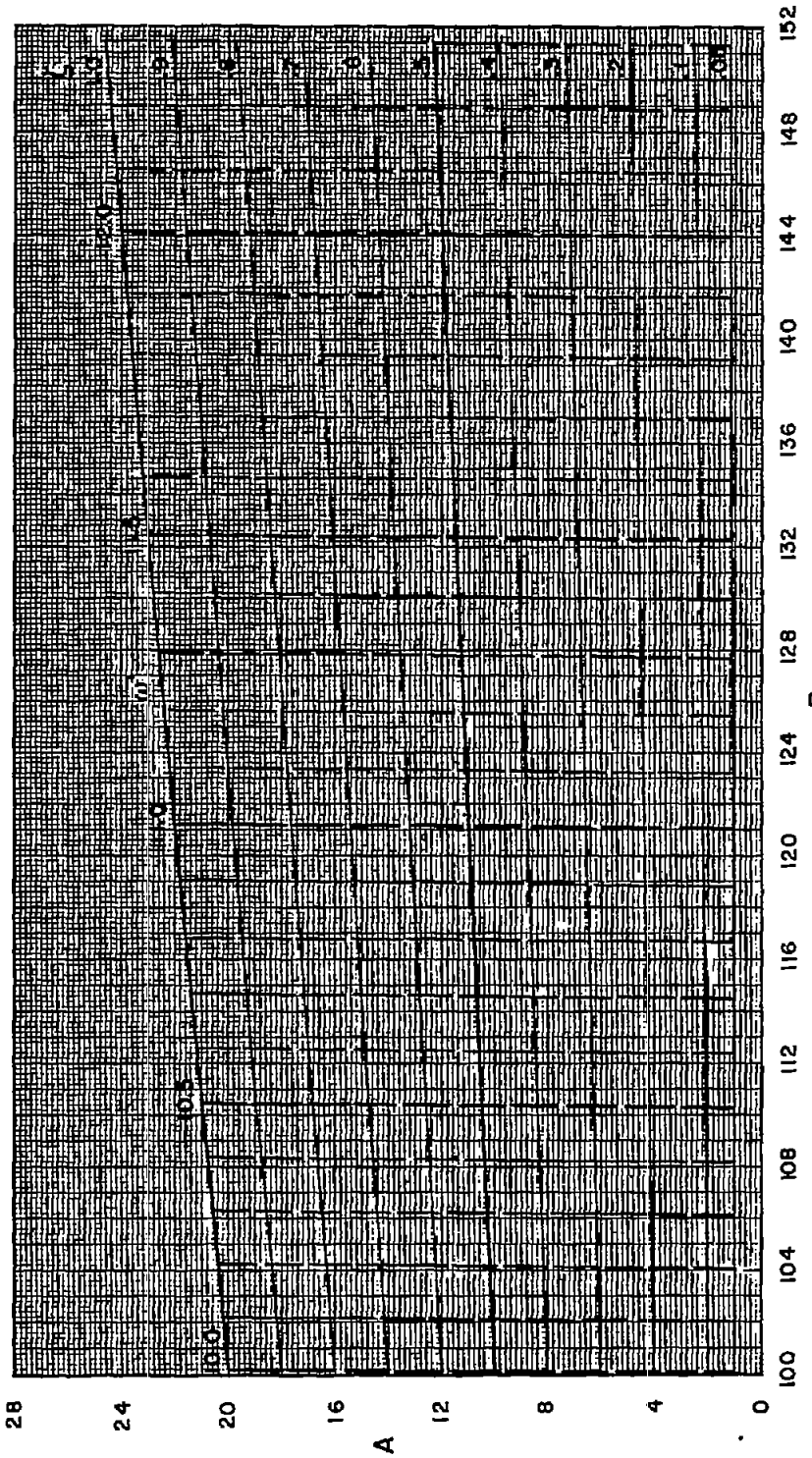

(c) $100 < B < 152$.

Figure 7.- Continued.

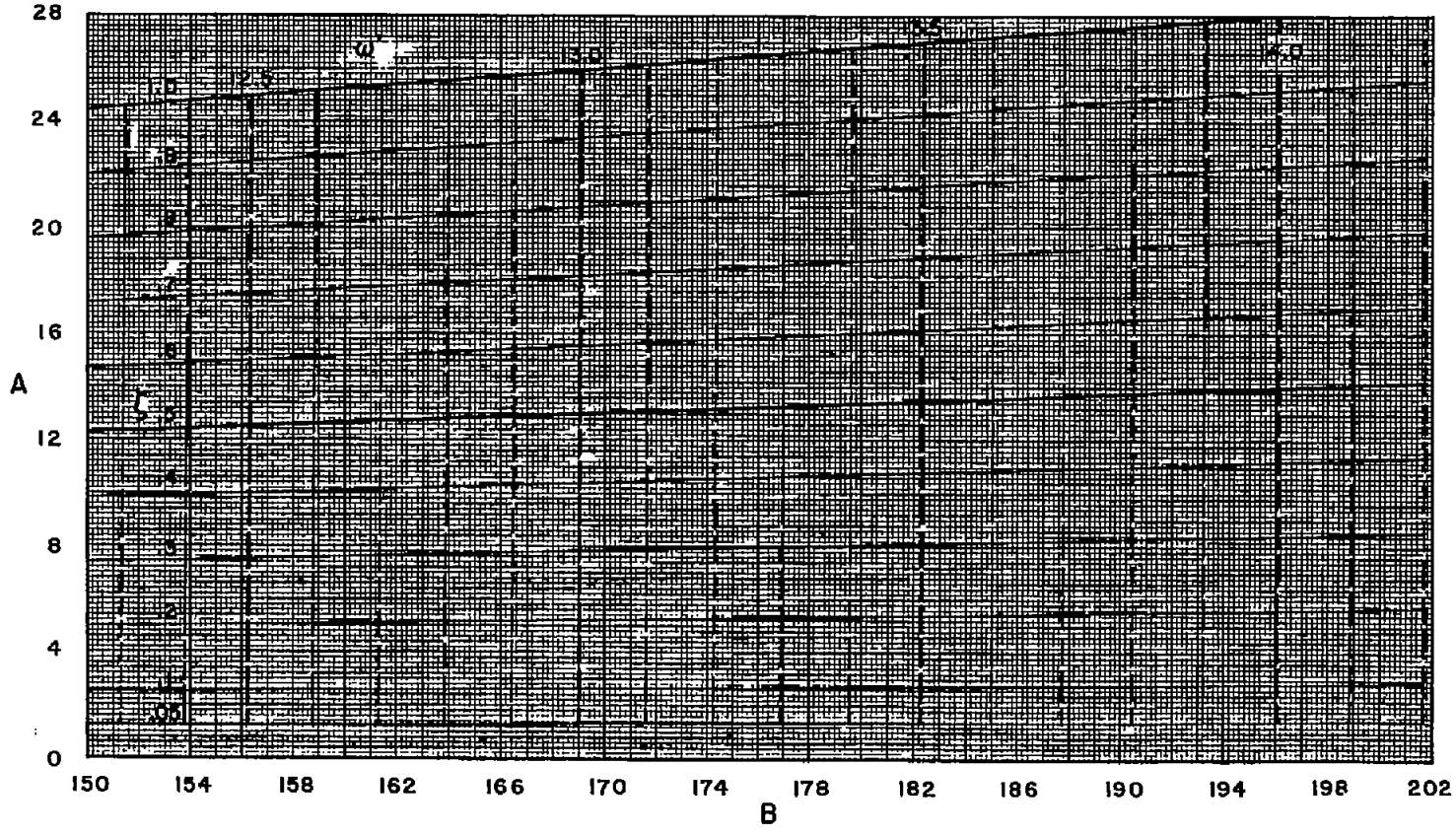

(d) $150 < B < 202$.

Figure 7.- Concluded.

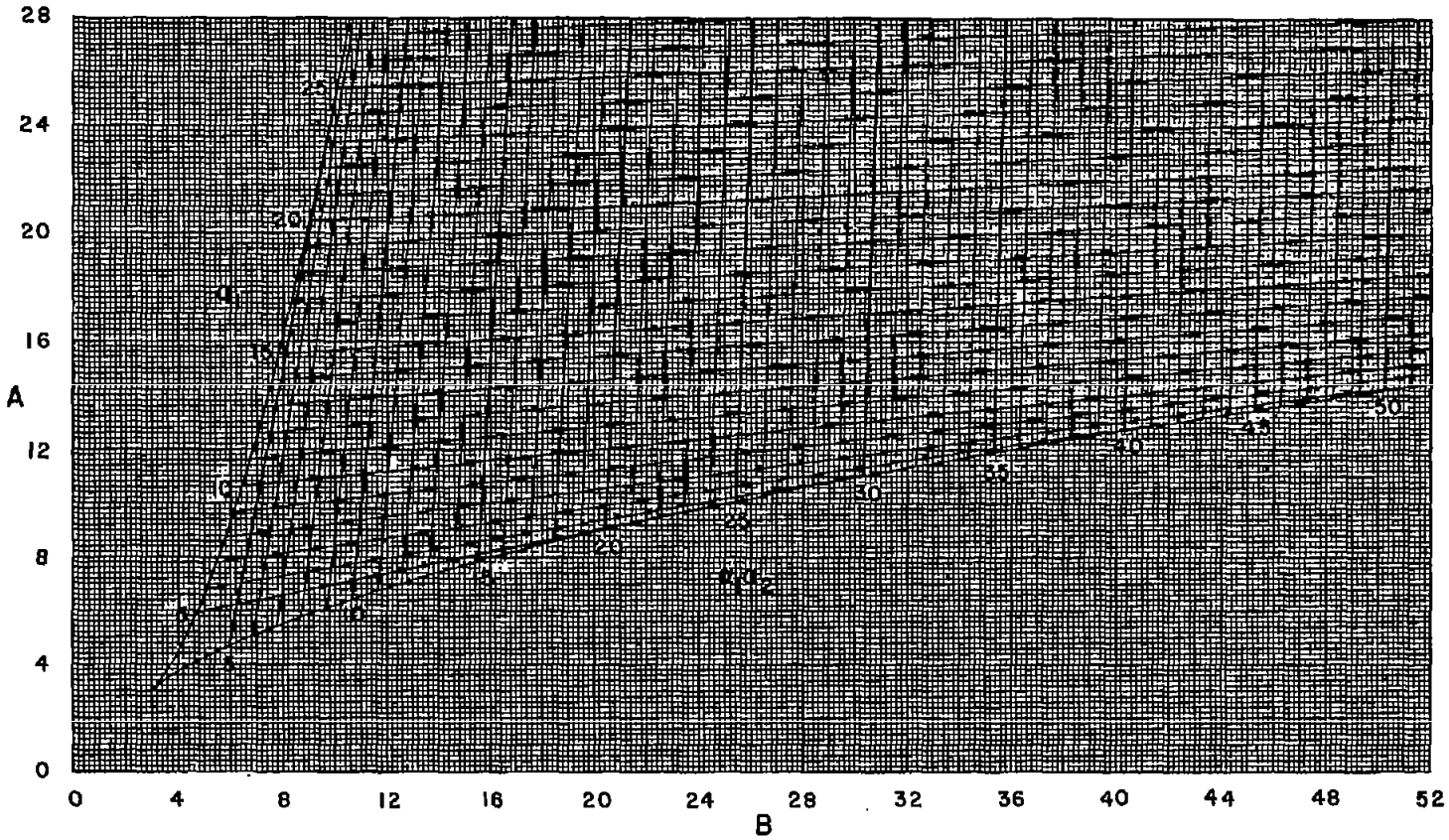

(a) $0 < B < 52$.

Figure 8.- Root charts for the normalized cubic equation when $\zeta > 1$.

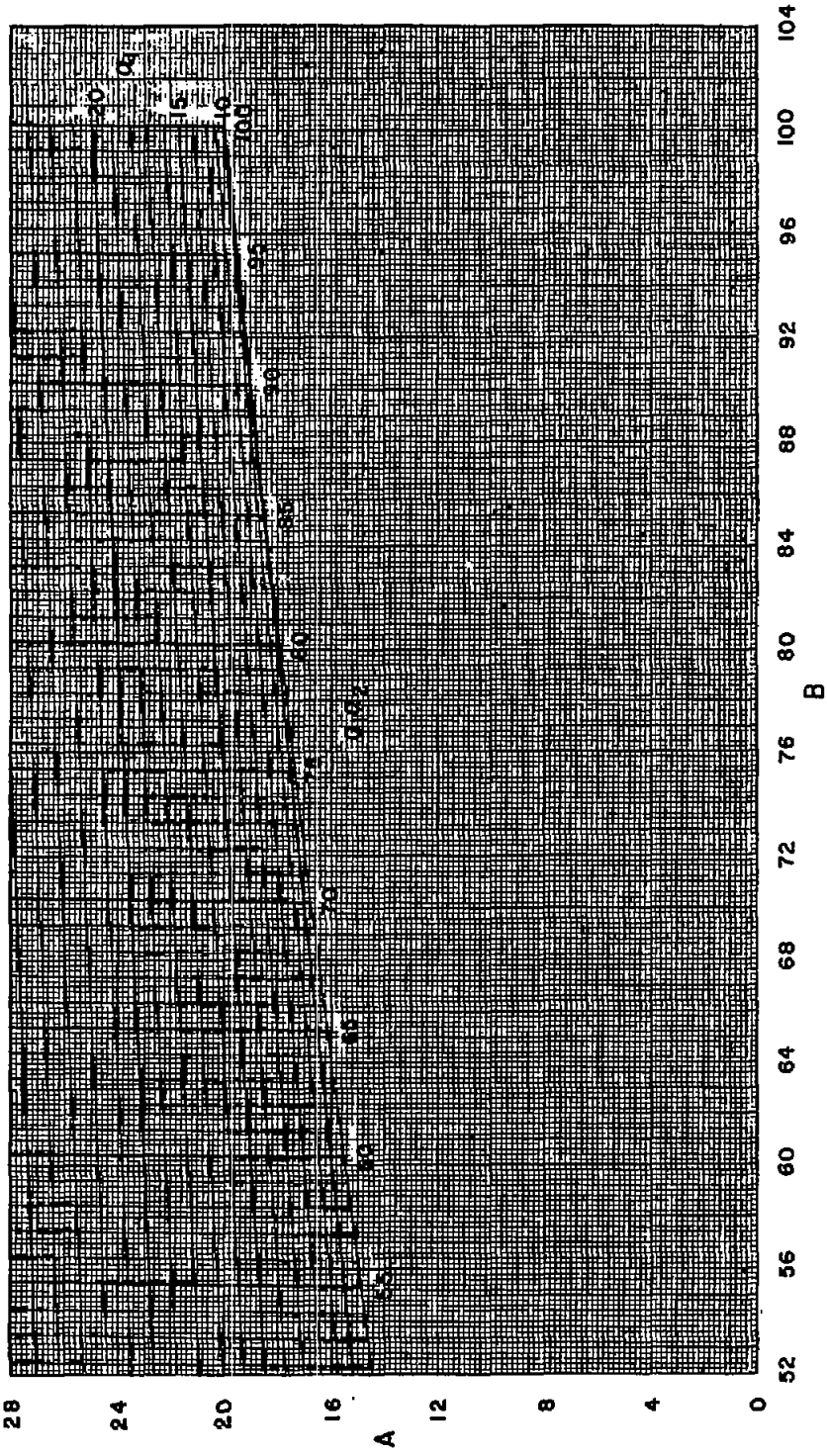

(b) $50 < B < 102$.

Figure 8.- Continued.

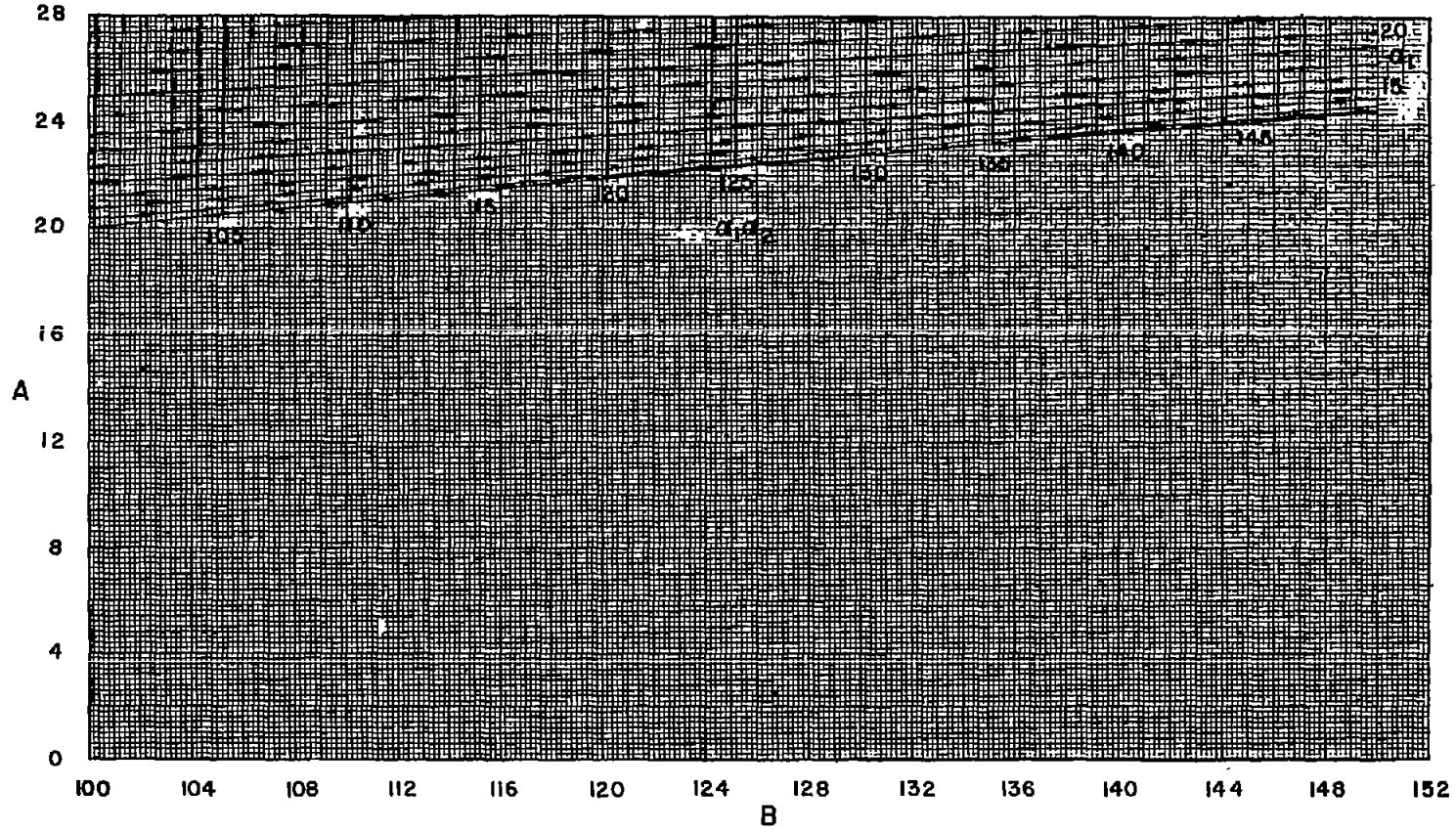

(c) $100 < B < 152$.

Figure 8.- Concluded.

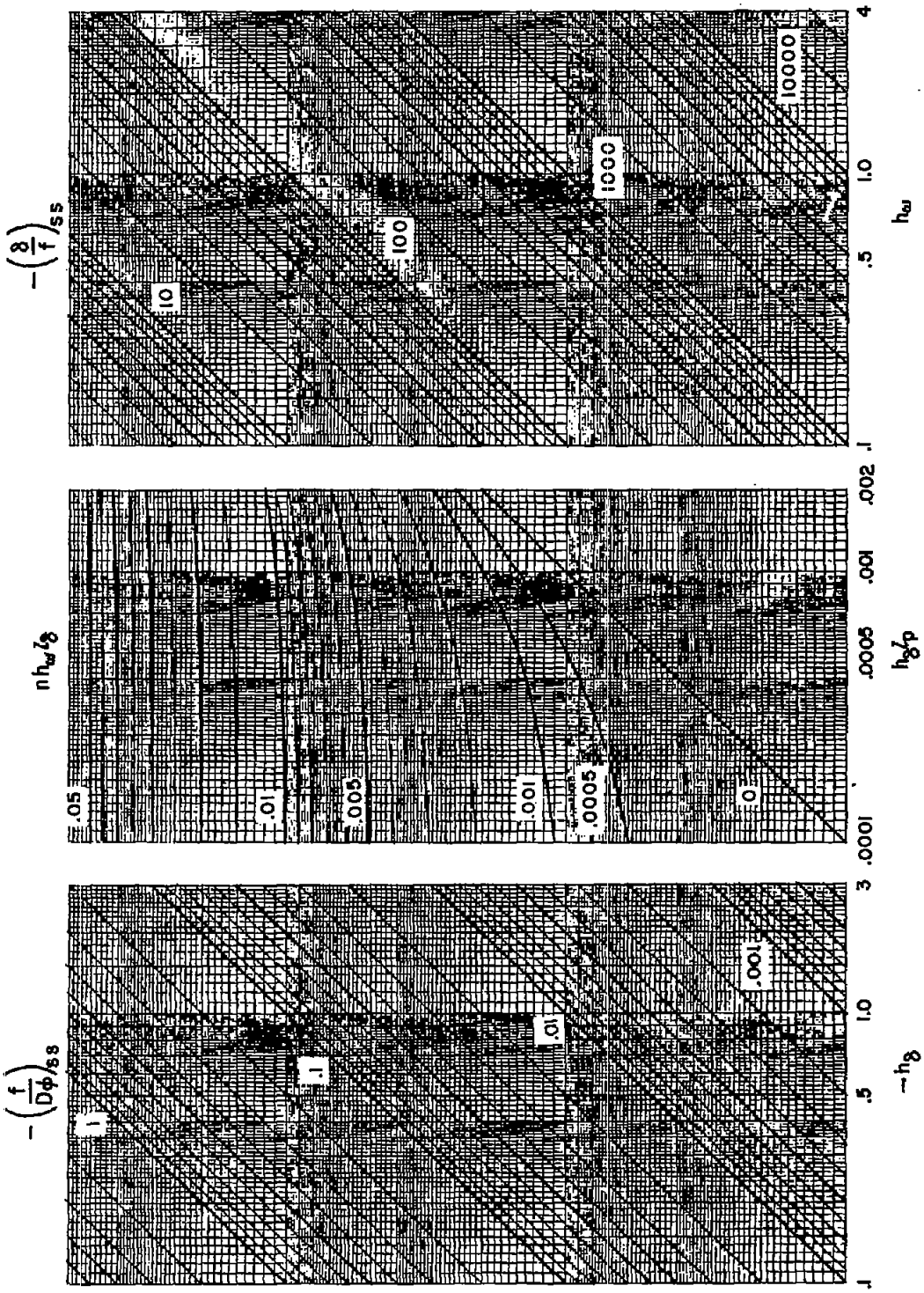

Figure 9.- Rolleron steady-state chart.